Calhoun
Institutional Archive of the Naval Postgraduate School

Calhoun: The NPS Institutional Archive

DSpace Repository

Theses and Dissertations | 1. Thesis and Dissertation Collection, all items

1990-12

Characteristics of sound radiation from large raindrops

Snyder, David Eugene

Monterey, California: Naval Postgraduate School

http://hdl.handle.net/10945/27674

This publication is a work of the U.S. Government as defined in Title 17, United States Code, Section 101. Copyright protection is not available for this work in the United States.

Downloaded from NPS Archive: Calhoun

http://www.nps.edu/library

Calhoun is the Naval Postgraduate School's public access digital repository for research materials and institutional publications created by the NPS community. Calhoun is named for Professor of Mathematics Guy K. Calhoun, NPS's first appointed -- and published -- scholarly author.

Dudley Knox Library / Naval Postgraduate School
411 Dyer Road / 1 University Circle
Monterey, California USA 93943

AD-A246 246

NAVAL POSTGRADUATE SCHOOL

Monterey, California

DTIC
ELECTE
FEB 21 1992
S B D

THESIS

Characteristics of Sound Radiation from Large Raindrops

by

Lieutenant David Eugene Snyder

December 1990

Thesis Advisor: H. Medwin
Co-advisor: J.A. Nystuen

Approved for public release; distribution unlimited.

92-04358

92 2 19 050

Jnclassified

Security Classification of this page

REPORT DOCUMENTATION PAGE

1a Report Security Classification Unclassified		1b Restrictive Markings	
2a Security Classification Authority		3 Distribution Availability of Report	
2b Declassification/Downgrading Schedule		Approved for public release; distribution is unlimited	
4 Performing Organization Report Number(s)		5 Monitoring Organization Report Number(s)	
6a Name of Performing Organization Naval Postgraduate School	6b Office Symbol *(If Applicable)* PH/Md	7a Name of Monitoring Organization Naval Postgraduate School	
6c Address *(city, state, and ZIP code)* Monterey, CA 93943-5000		7b Address *(city, state, and ZIP code)* Monterey, CA 93943-5000	
8a Name of Funding/Sponsoring Organization	8b Office Symbol *(If Applicable)*	9 Procurement Instrument Identification Number	
8c Address *(city, state, and ZIP code)*		10 Source of Funding Numbers	
		Program Element Number / Project No / Task No / Work Unit Accession No	

11 Title *(Include Security Classification)* CHARACTERISTICS OF SOUND RADIATION FROM LARGE RAINDROPS

12 Personal Author(s) Snyder, David E.

13a Type of Report	13b Time Covered	14 Date of Report *(year, month,day)*	15 Page Count
Master's Thesis	From To	December 1990	53

16 Supplementary Notation The views expressed in this thesis are those of the author and do not reflect the official policy or position of the Department of Defense or the U.S. Government.

17 Cosati Codes			18 Subject Terms *(continue on reverse if necessary and identify by block number)*
Field	Group	Subgroup	raindrops, ambient noise, acoustic radiation from bubbles, raindrop size distribution, underwater sound spectrum

19 Abstract *(continue on reverse if necessary and identify by block number)*

Drop diameters from 2.7mm to 4.6mm are common in heavy rainfall. The impact and bubble signals of the underwater sound radiation from these large drops at their terminal velocities have been identified. At a 1 MHz sampling rate,several notches are observed in the approximately 100 μs duration impact signal. These notches with time separations of 3 to 4 μs between peak and trough, are shown to be caused by internal drop reflections of the impact pressure wave. Frequently observed low frequency oscillations from 2 to 10 kHz, which lag the impact signal by 40 to 55 ms, are attributed to bubbles formed by a complex jet mechanism which has been identified by high speed photography. This mechanism is unlike the bubble formation mechanism for drops of .8 to 1.1 mm diameter previously reported in the literature. Both the frequency of the bubble oscillation and the time lag are functions of drop size. The percentage of drops that generate bubbles is shown to be a function of drop size as well. This percentage peaks at 65% for drops of approximately 4 mm diameter and there are essentially no bubbles for drop sizes in the range of 1.2 to 2 mm in diameter. Although the amplitudes of the impact and bubble signals are often comparable, the acoustic energy radiated by the bubble is greater due to its longer time duration. These results suggest that it may be possible to determine the number of drops as a function of diameter from the underwater sound spectrum of rainfall at sea.

20 Distribution/Availability of Abstract	21 Abstract Security Classification	
[X] unclassified/unlimited [ ] same as report [ ] DTIC users	Unclassified	
22a Name of Responsible Individual Herman Medwin	22b Telephone *(Include Area code)* (408) 624 1775	22c Office Symbol PH/Md

DD FORM 1473, JUN 86 *Previous editions are obselete.* SECURITY CLASSIFICATION OF THIS PAGE

S/N 0102-LF-014-6603 Unclassified

Approved for public release; distribution is unlimited

Characteristics of Sound Radiation from Large Raindrops

by

David Eugene Snyder
Lieutenant, U.S. Navy
B.S.E.E., United States Naval Academy, 1983

Submitted in partial fulfillment of the
requirements for the degree of

MASTER OF SCIENCE IN
ENGINEERING ACOUSTICS

from the

NAVAL POSTGRADUATE SCHOOL

December 1990

Author: [redacted]

David Eugene Snyder

Approved by: [redacted]

H. Medwin, Advisor

[redacted]

J.A. Nystuen, Co-Advisor

[redacted]

Anthony A. Atchley
Engineering Acoustics Academic Committee

ABSTRACT

Drop diameters from 2.7 mm to 4.6 mm are common in heavy rainfall. The impact and bubble signals of the underwater sound radiation from these large drops at their terminal velocities have been identified. At a 1 MHz sampling rate, several notches are observed in the approximately 100 μs duration impact signal. These notches with time separations of 3 to 4 μs between peak and trough, are shown to be caused by internal drop reflections of the impact pressure wave. Frequently observed low frequency oscillations from 2 to 10 kHz, which lag the impact signal by 40 to 55 ms, are attributed to bubbles formed by a complex jet mechanism which has been identified by high speed photography. This mechanism is unlike the bubble formation mechanism for drops of .8 to 1.1 mm diameter previously reported in the literature. Both the frequency of the bubble oscillation and the time lag are functions of drop size. The percentage of drops that generate bubbles is shown to be a function of drop size as well. This percentage peaks at 65% for drops of approximately 4 mm diameter and there are essentially no bubbles for drop sizes in the range of 1.2 to 2 mm in diameter. Although the amplitudes of the impact and bubble signals are often comparable, the acoustic energy radiated by the bubble is greater due to its longer time duration. These results suggest that it may be possible to determine the number of drops as a function of diameter from the underwater sound spectrum of rainfall at sea.

Accession For
NTIS GRA&I ☑
DTIC TAB ☐
Unannounced ☐
Justification
By
Distribution/
Availability Codes
Dist | Avail and/or Special
A-1

TABLE OF CONTENTS

I. BACKGROUND 1

II. DETERMINATION OF TERMINAL VELOCITY 8

A. EXPERIMENT 8

1. The Stroboscope Technique 8

2. The High Speed Photographic Technique 9

B. RESULTS 9

III. ACOUSTICAL EXPERIMENT 14

A. EXPERIMENT 14

B. IMPACT CHARACTERISTICS 17

C. BUBBLE CHARACTERISTICS 18

D. SPECTRAL CHARACTERISTICS OF THE ACOUSTICAL SIGNATURE 22

IV. HIGH SPEED PHOTOGRAPHY EXPERIMENT 28

V. CONCLUSIONS 33

APPENDIX A - HIGH SPEED MOTION ANALYSIS OF A WATER DROP 35

LIST OF REFERENCES 41

INITIAL DISTRIBUTION LIST 43

LIST OF TABLES

2.1 DROP SIZE AND TERMINAL VELOCITY 11

LIST OF FIGURES

1.1 The prediction of the effect of wind on the underwater sound generated by light rain superimposed onto field observations. (from Nystuen, 1990) 3

1.2 Raindrop size distribution for several rainfall rates 5

1.3 Comparison of $V_T = c\, a^{\frac{1}{2}}$ fit with terminal velocity data from Table 2.1 7

2.1 Terminal Velocity Experimental Setup (Side View) 10

2.2 Terminal Velocity Experimental Setup (Top View) 10

2.3 Experimental Terminal Velocity Data Plotted on Theoretical Curves . 12

3.1 Acoustical experiment setup (Side View) 16

3.2 Acoustical experiment setup (Top View) 16

3.3 Typical impact signal 18

3.4 Impact signal from 4.6 mm drop 19

3.5 Sketch of 4.6 mm drop profile 19

3.6 Bubble signal from 4.6 mm drop 20

3.7 Bubble delay time 21

3.8 Bubble Creation Percentage (% Drops with Bubbles vs. Drop Diameter) 22

3.9 Typical Impact Spectrum (2-300 kHz) 24

3.10 Typical Impact Spectrum (2-100 kHz) 24

3.11 Typical Bubble Spectrum (2-20 kHz) 26

3.12 Dominant Bubble Frequency vs. Drop Diameter 26

3.13 Bubble Frequency vs. Drop Kinetic Energy 27

4.1 Drop Sequence Sketch 32

ACKNOWLEDGMENTS

It would be impossible to list everyone who has contributed to the completion of this thesis without missing someone. I feel obligated, however, to thank those individuals whose time, effort and support were key to accomplishing this research. First and foremost, I wish to thank my lab partner Pete Jacobus without whom, quite literally, this thesis could not have been done. I also wish to thank Professor Medwin and Professor Nystuen for their wisdom and guidance in this effort and my wife, Lynne, for her patience and support. Finally, a heartfelt thanks for the enthusiasm and professionalism displayed by Mark Mattivi and Dominic Hart of Brooks Institute, who provided technical support for the high speed photography needed to cap this thesis research.

I. BACKGROUND

For several years meteorologists and other atmospheric scientists have been searching for a solution to the problem of measuring rainfall rate at sea. Several methods thought to hold great promise involve the use of measurements from satellites (using visible, infrared, passive and active microwave wavelengths). These techniques all suffer from the lack of surface measurements for verification and several (the visible and infrared techniques) merely infer precipitation from the presence of clouds. A new idea is to measure rainfall rate by passively monitoring the underwater sound generated by rain drops splashing the ocean surface. This acoustical measurement has the potential of providing the needed surface verification for the satellite data.

For many years rain has been known to generate underwater sound (Heindsman, et al., 1955), but only in recent years has an attempt been made to correlate rainfall rate with underwater sound levels from rain (Nystuen, 1986). This recent work added support for the idea of acoustical rainfall rate measurement while pointing out deficiencies in the understanding of the mechanisms by which raindrops produce underwater sound. Follow-on field studies of a similar nature have suggested a significant effect of wind speed on the amount of sound generated by light rain (Scrimger, et al., 1987, 1989). The addition of this variable to the problem serves to add to the complexity of quantifying rainfall rate. Nevertheless, the acoustical detection of precipitation has been demonstrated for oceanic conditions with wave heights of up to four meters and wind speeds up to 20 m/s (Nystuen and Farmer, 1989).

The first step in quantifying rainfall rate from underwater sound is to understand how that sound is generated and, in particular, how individual drops generate underwater sound. In addition, one must understand how the generation of that sound is affected by wind speed and the physical characteristics of the surface of the water. In order to isolate sound production due to rain from other ambient noise present at sea and from interactive effects due to the presence of multiple raindrops, a controlled experimental environment is essential. Experimental observations for drops which do not simulate rain (i.e., non-terminal velocity drops) are of little consequence for the study of rain at sea.

The first published experimental study of sound generated by drop splashes (Franz, 1959) showed that there are essentially two components to the generation of sound by a drop. The first is the initial impact of the drop on the water's surface and the second is the damped oscillation of a bubble produced after impact (if a bubble is produced) and trapped under the water's surface. Recent experiments (Pumphrey, et al., 1989) and theoretical studies (Longuet-Higgins, 1990; Oguz and Prosperetti, 1990) have demonstrated that for drops impacting the water surface at normal incidence, there is a range of drop sizes that always produce bubbles underwater. The size range of terminal velocity drops that produce bubbles with 100% occurrence is 0.8-1.1 mm diameter. The bubble produced by drops of this size has a characteristic frequency centered around 15 kHz. Drops of this range are almost always present in rain even if the rain is very light. When bubbles are present, they generate two orders of magnitude more underwater acoustic energy than impacts. Therefore, light rain with no wind is capable of producing significant underwater sound levels if 0.8-1.1 mm diameter drops are present.

Naturally, at sea, wind is almost always present. Wind causes drops to impact the water surface at oblique angles rather than normal. Kurgan (1989) studied

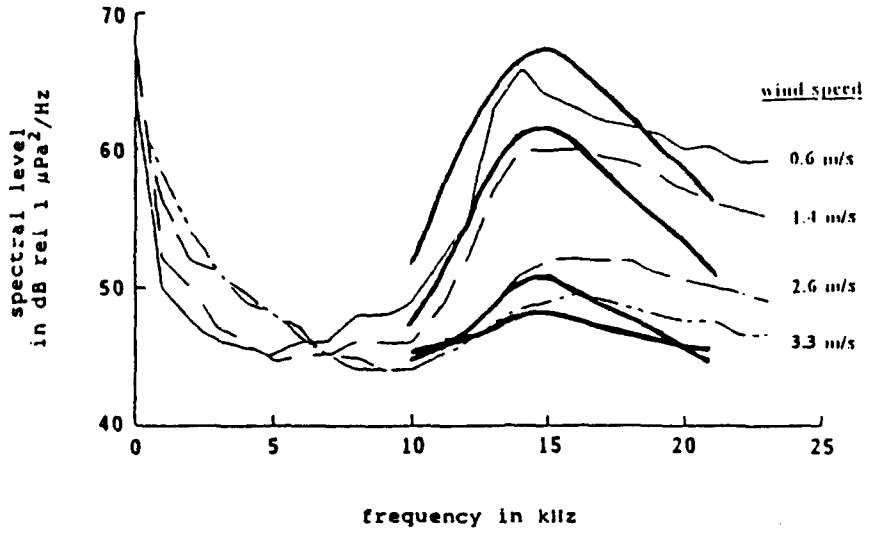

Figure 1.1: The prediction of the effect of wind on the underwater sound generated by light rain superimposed onto field observations. (from Nystuen, 1990)
Heavy solid lines indicate spectral predictions. The reduction in spectral level is attributed to a reduction in the probability of bubble production by raindrops impacting at oblique angles.

the effect of oblique incidence for small terminal velocity drops (Medwin, et al., 1990). As the angle of incidence increases, the probability of bubble production is reduced from 100% at normal incidence to near 0% at angles exceeding 25° (from the normal) for 0.8-1.1 mm drops. The increase of wind speed which will cause this change in incidence angle is from 0 m/s to 3 m/s. Figure 1.1 (from Nystuen, 1991) demonstrates that the effect of wind on the spectral level of sound from light rain can be predicted based on the reduction in the probability of bubble production for 0.8-1.1 mm drops.

As evidenced by the preceding discussion, extensive research on these small drops (< 2 mm diameter) has lead to the following conclusions regarding the measurement of rainfall rate. First, for light wind conditions ($\leq$ 3 m/s), the acoustic energy of bubbles produced by 0.8-1.1 mm drops dominates the sound field particularly near 15 kHz. However, since wind and ocean roughness add other variables to the function of bubble production by these drops, there is a poor correlation between sound field and rainfall rate. For wind speeds higher than 3 m/s, the impact sound becomes, relatively, more significant. Since impact sound level is proportional to drop kinetic energy, it is well correlated with rainfall rate (Ulbrich and Atlas, 1978). In any event, the ability (if it exists) to predict light rainfall rate (mm/hr) from the sound field is of dubious worth since most rain volume, particularly at sea, is due to heavier rain containing large raindrops (2-5 mm diameter). Little was known about the acoustical characteristics of sound generated by these larger drops impacting at terminal velocity until the research for this thesis was accomplished.

Figure 1.2 shows raindrop size distribution from data recorded during a convective storm at Clinton Lake, IL. in October 1982 (courtesy J. Nystuen). These are typical distributions which have been shaded to indicate two regions of interest for underwater sound production by rain. The narrow shaded region on the left contains what will henceforth be referred to as Type I raindrops (0.8-1.1 mm diameter). This region has been studied extensively and is reponsible for underwater sound generation by light rain. Note that these drop sizes are present in almost all rain, including the lightest recorded (0.6 mm/hr). The wide region on the right contains drop diameters 2.7-4.6 mm and will be denoted as Type II raindrops. This is the range of drops investigated and reported on in this thesis. The lower limit (2.7 mm diameter) for Type II drops will be explained later. The upper limit (4.6 mm) is the largest diameter commonly observed.

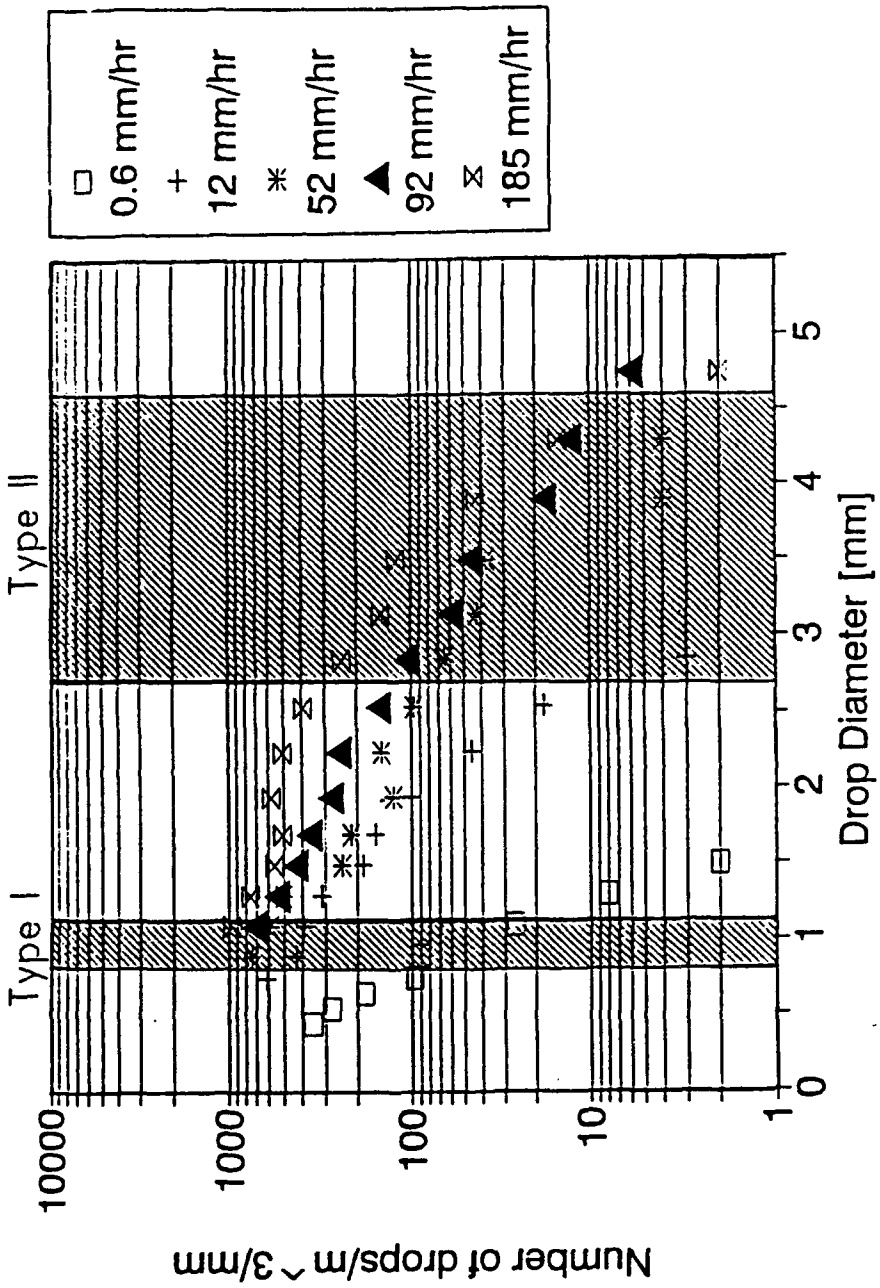

Figure 1.2: Raindrop size distribution for several rainfall rates

The importance of these Type II raindrops is demonstrated by a quantitative analysis of their relative contribution to rainfall rate (RR).

$$RR = \int_0^\infty (\text{DSD})\, V_T\, a^3\, da \tag{1.1}$$

where

- DSD $\equiv$ drop size distribution, [# of drops/m^3 mm]
- V_T = terminal velocity, [m/s]
- a = drop radius, [mm]

Assuming $V_T = c\, a^{\frac{1}{2}}$, (see Figure 1.3) where c is a proportionality constant, gives

$$RR = A \int_0^\infty (\text{DSD})\, a^{\frac{7}{2}}\, da \tag{1.2}$$

which shows that rainfall rate is a high moment of the DSD and therefore, large drops are the most important of the drops in a given distribution.

Based on the preceding analysis and consideration of the rainfall distributions in Figure 1.2, it is evident that for rainfall rates in excess of 12 mm/hr, Type II drops make up a significant portion of the water mass.

For the sake of completeness, it should be mentioned that Pumphrey and Crum (1989), and Oguz and Prosperetti (1990), both present data for drops within the 2-5 mm diameter size range. However, all of that research was done for drops impacting the water at velocities well below terminal velocity. The assumption that non-terminal velocity drops were acceptable to simulate rainfall in the 2-5 mm size range was unfortunate and has proven to be quite erroneous. The results which follow in Chapters III and IV will show that the formation of a conical cavity as reported by the aforementioned researchers and the subsequent pinch-off of a drop at the apex of the cone by capillary wave action is not the actual mechanism of bubble production for Type II raindrops at terminal velocity.

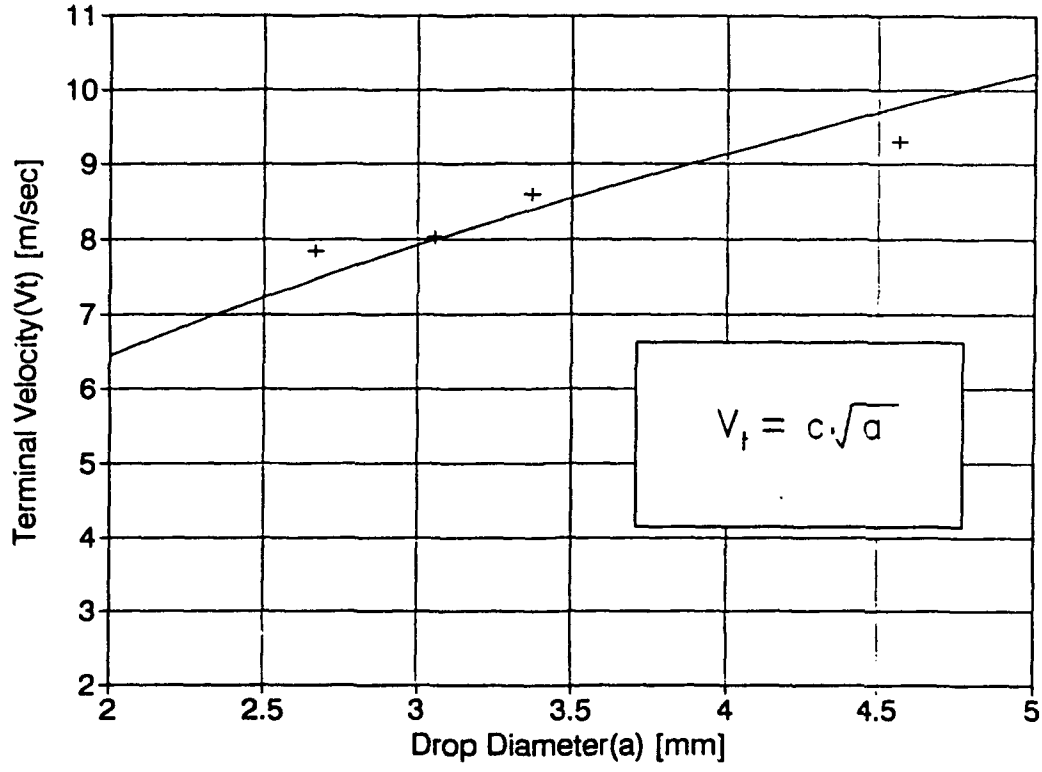

Figure 1.3: Comparison of $V_T = c\, a^{\frac{1}{2}}$ fit with terminal velocity data from Table 2.1

II. DETERMINATION OF TERMINAL VELOCITY

A. EXPERIMENT

1. The Stroboscope Technique

In order to validate the assumption that the drops used in this experiment simulate rain, it was first necessary to demonstrate that drops of the desired size would impact the water surface at their terminal velocities. This was accomplished optically using the setup shown in Figures 2.1 and 2.2.

The drop images were recorded using a SONY CCD-V99 video camera recorder. The camera was positioned 2.6 meters away from a grid, suspended over the tank as shown in Figure 2.1. This position was optimum for obtaining the maximum depth of field while maintaining an adequate field of view. The grid of horizontal lines was constructed using a wood frame with white fly line strung across at two centimeter intervals. The thickness and color of the fly line allowed the grid to show up clearly against a black backdrop.

Illumination for the experiment was provided by three GenRad Strobotacs, Type 1531-AB, positioned as shown in Figures 2.1 and 2.2. The strobotacs were slaved to each other with one master to ensure simultaneous triggering. The two strobes mounted on the tank illuminated a point ten centimeters in front of the horizontal grid (i.e., toward the camera). They were separated from each other and the video camera by approximately 120 degrees, as shown in Figure 2.2. This positioning was crucial to obtaining images of the drops on video tape. Since water droplets forward scatter light more effectively than they backscatter, it is desirable to backlight the drops. Direct backlighting is impossible in this situation because

it would wash out the video imagery. The position as shown represents a trade-off between these two effects. The third strobe was positioned above and to the side of the camera and shone directly on the horizontal grid to illuminate it.

The strobe rate setting for all drop sizes was 333 flashes per second. This rate was selected to ensure that the largest (highest velocity) drops would be illuminated by the strobe at least eight times between the top and bottom of the camera field of view. The frame speed of the CCD-V99 video camera is 1/30 second. The shutter speed selected (1/60 second) was the slowest setting available. This setting gave the highest probability of having an open shutter condition as the drop was passing through the field of view, and resulted in successfully obtaining 3-5 drop images for most drops. The camera was carefully positioned to ensure that the camera axis was perpendicular to the grid plane.

The velocity of each drop was determined by measuring the physical separation of successive images against a vertically positioned grid with horizontal lines in the background. The average separation was divided by strobe rate to obtain velocity.

2. The High Speed Photographic Technique

Another method of terminal velocity verification became available as a result of the high speed photography which is discussed in detail later. Drop velocity was calculated knowing the frame speed of the camera and measuring the fall distance between consecutive frames.

B. RESULTS

The results of the experiment discussed above are tabulated in Table 2.1 below. The data are plotted on a reproduction of a set of theoretical curves of terminal velocity vs. drop diameter (Pruppacher and Klett, 1978). Drops of a given diameter

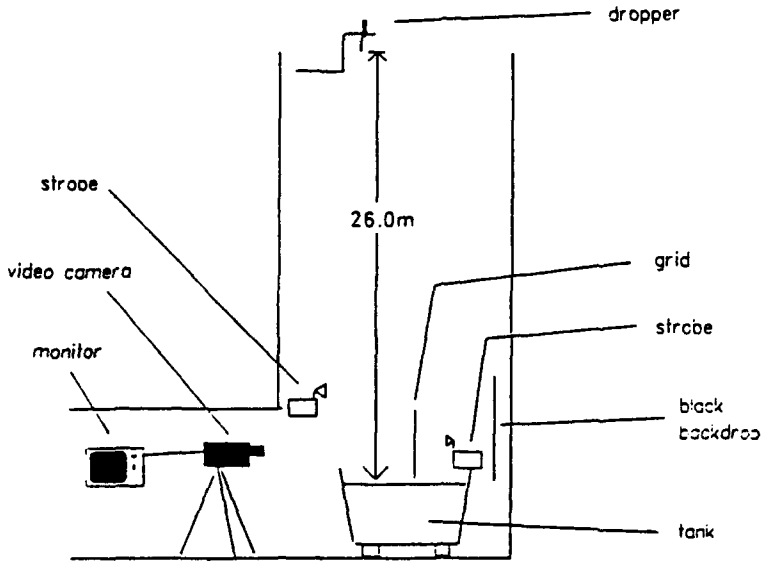

Figure 2.1: Terminal Velocity Experimental Setup (Side View)

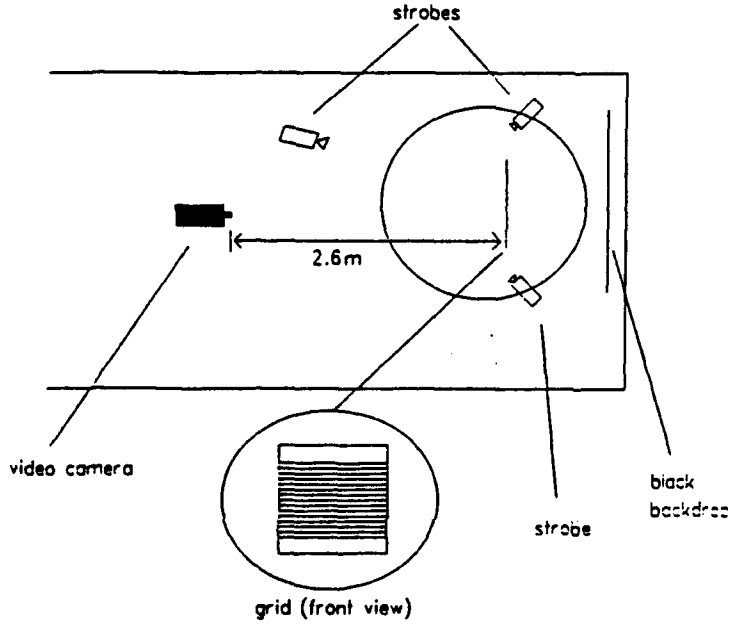

Figure 2.2: Terminal Velocity Experimental Setup (Top View)

TABLE 2.1: DROP SIZE AND TERMINAL VELOCITY

Drop Size Diameter [mm]	Experimental Velocity [m/s]	Theoretical Velocity [m/s]	Percent Deviation [%]
2.67	7.8 ± .1	7.7	1.3
3.06	8.0 ± .2	8.1	1.2
3.37	8.6 ± .4	8.5	1.2
4.57	9.3 ± .2	9.1	2.2

were made using methods discussed in the first section of Chapter III. The fit of these data points closely follows the theoretical curves. The velocity of various size drops was then plotted against theoretical predictions as shown in Figure 2.3. A second and perhaps more intuitive method of verifying terminal velocity was noting that, for a given drop size, the vertical spacing between drop images had a variance of 1-3%, indicating essentially equal spacing and thus constant velocity. Much of the small variance was due to taking vertical spacing measurements from a video image displayed on a curved video monitor screen.

Drop velocity for 4.6 mm diameter drops was also determined using high speed photography. The drop velocity measured in this manner was 8.6 ± .4 m/s. This is lower than expected. This suggests that the frame speed of the high speed camera was higher by approximately 20 frames/sec (5%) than the dial setting of 400 frames/sec.

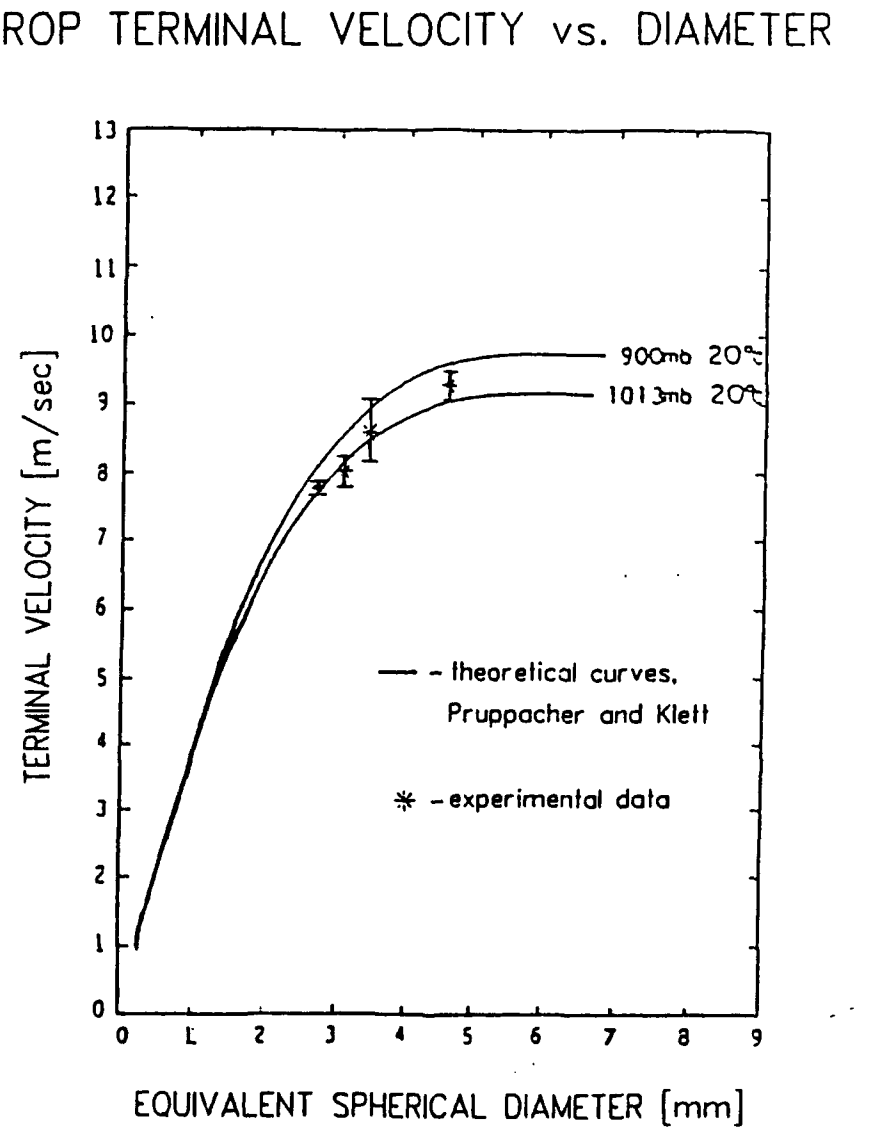

Note: Average atmospheric pressure for experimental data – 1017.5mb

Figure 2.3: Experimental Terminal Velocity Data Plotted on Theoretical Curves

Based on uniform drop image spacing, comparison of calculated with theoretical terminal velocity and corroboration using the high speed photography measurements, it was determined that all drop sizes of interest were reaching terminal velocity prior to impacting the water surface in the tank.

III. ACOUSTICAL EXPERIMENT

A. EXPERIMENT

The experimental setup used to measure the acoustical signature of individual large drops hitting the water surface at normal incidence is shown in Figures 3.1 and 3.2.

The range of drop sizes used was from 2.7 mm to 4.6 mm in diameter. To obtain the desired drop sizes, several drop forming devices were used. For the 2.7 mm drops, which correspond to a volume of 10 μL, an Eppendorf digital pipette Model 4710 was used with a range 0.5-10 μL. At the 10 μL drop size, this pipette's published volume accuracy is $\pm 1\%$. For drop diameters corresponding to volumes of 15, 20 and 25 μL, an Eppendorf pipette with a range of 10-100 μL was used. The volume accuracy for these sizes was $\pm 1\%$. For drop diameters corresponding to 32.5, 40 and 50 μL, three individually calibrated glass eye droppers were used. The accuracy for these sizes was judged to be no more than $\pm 5\%$ based on measuring the total volume for 50 drops collected in a graduated cylinder. Use of the glass eye droppers was necessitated by the fact that drops with volumes greater than 25 μL tended to detach prematurely from the tip of the 10-100 μL pipette. The glass droppers with rounded, more bulbous tips gave the larger drops more surface area to cling to prior to reaching full size.

When a drop impacted the water surface, the impact point relative to a point on the surface directly above the hydrophone was recorded on video. This distance was determined by using a pair of dividers to measure the relative distance between

impact point and hydrophone on the video monitor screen. This relative measurement was converted to an absolute one utilizing a meter stick placed in the field of view just above the water surface. The position, distance and angle were needed to calculate the on axis pressure amplitude at range 1 m by assuming dipole radiation from the source.

The hydrophone, similar to an LC-5 type hydrophone, was constructed from two $\frac{1}{8}$ inch coaxial cylindrical barium titanate elements. It was calibrated by the reciprocity method prior to the experiment. This calibration showed the hydrophone to have a flat response ($\pm$ 3.0 db) over a frequency range of 5 to 300 kHz. The hydrophone was positioned approximately in the center of the tank at a depth of 15 cm. The center position was chosen to minimize the interference of tank wall reverberation with the signal of interest. The hydrophone depth was selected to maximize acoustical signal strength while still maintaining enough distance from the impact point to mitigate hydrodynamic effects on the hydrophone and to ensure the hydrophone was in the acoustical far-field of the bubble. This shallow depth selection also, incidentally, helped to reduce interference from tank bottom reverberation. The signal voltage from the hydrophone was amplified by a PAR 113 Pre-Amplifier with a gain of 2000. It was then passed through a Krohn-Hite 3202R band pass filter and a Krohn-Hite 3322 band pass filter, giving a total roll-off of 48 dB/octave. Finally the signal was processed using an R.C. Electronics Computerscope Analog to Digital converter installed in an IBM XT personal computer. Filter settings for the low end of the bandwidth varied throughout the experiment from 1 to 4 kHz due to daily changes in the noise floor. The upper band frequency was 30 kHz.

Two sample rates were used for analog to digital conversion of the acoustical signal. In order to obtain a signal of high resolution for the drop impact signal, an A/D sample rate of 1 MHz was selected. This was the maximum sample rate for

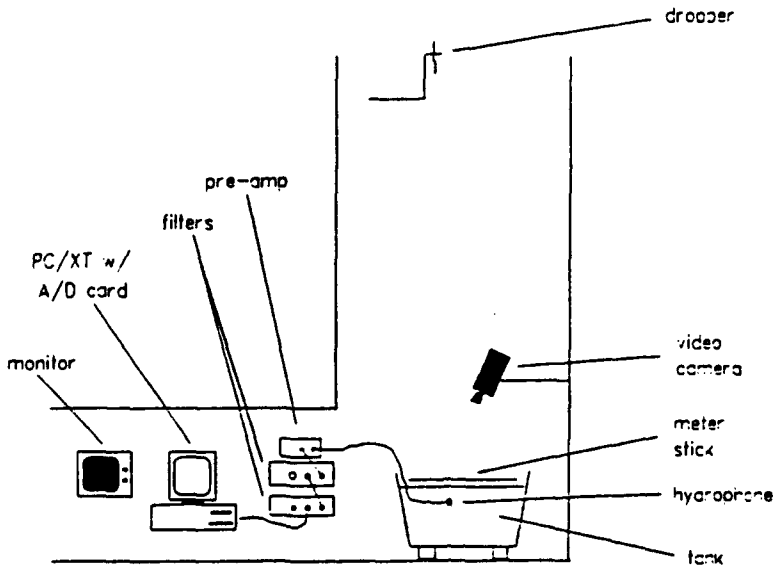

Figure 3.1: Acoustical experiment setup (Side View)

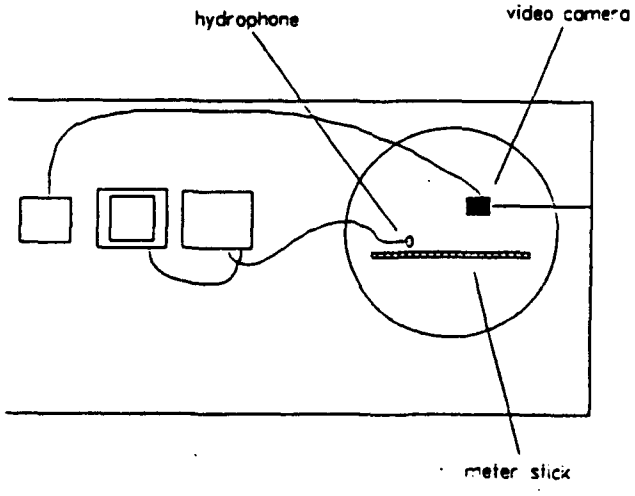

Figure 3.2: Acoustical experiment setup (Top View)

Computerscope. Due to buffer size limitations in the computer, it was not possible to maintain this maximum sample rate and still have a long enough time record to include both impact and bubble signal on the same data run. For this reason, a sample rate of 250 kHz was chosen for investigation of the later occurring bubble signal. This allowed the time record length to be extended sufficiently while still sampling at a rate well above the highest expected signal frequency, based on initial investigations at the 1 MHz sampling rate.

B. IMPACT CHARACTERISTICS

The maximum sampling rate was used to investigate impact signal characteristics due to the extremely short time duration of its acoustic signal (90-120 μs). Figure 3.3 shows a sketch of a typical impact for a relatively low sample rate, as published by previous researchers (Franz, 1959). This picture is in contrast to Figure 3.4, which shows data from a 4.6 mm diameter drop impact sampled at 1 MHz. By mentally super-imposing the image of the impact shown in Figure 3.4 on the image in Figure 3.3, it is apparent that the general shape of the signal in Figure 3.4 follows the shape of the pulse in Figure 3.3. However, it has notches at approximately 10 to 11 μs intervals modulating it. The explanation for these notches is that they are caused by interference between the pressure wave causing the characteristic impact signal by direct radiation (Figure 3.3) and a pressure wave reflected internally within the drop. There will be a 180° phase shift from reflection at the top of the drop. Figure 3.5 shows a sketch of a 4.6 mm diameter drop just prior to impact. The shape was determined by photographic methods discussed in Chapter IV. As shown, the vertical dimension of this drop is 3 mm, thus giving a round trip distance of 6 mm for an internal pressure wave reflecting off the top of the drop.

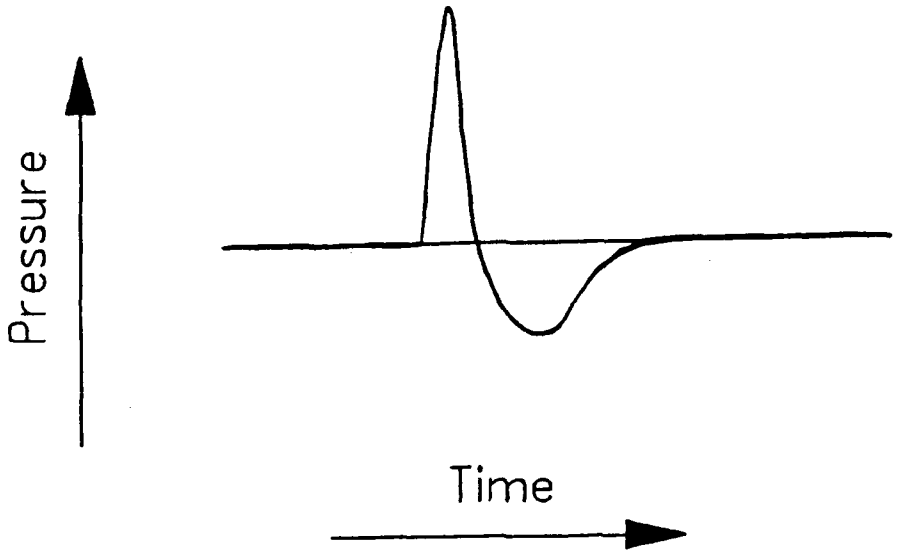

Figure 3.3: Typical impact signal

Using a standard value for speed of sound, the following travel time is calculated

$$t = \frac{2\,d}{c} = \frac{6 \times 10^{-6}\,m}{1500\,m/s} = 4.0\mu s \tag{3.1}$$

This calculated travel time matches well with the time (4.1 μs) between the peak of the impact signal and the first notch, as shown in Figure 3.4.

C. BUBBLE CHARACTERISTICS

Figure 3.6 shows the pressure vs. time signal of a bubble created by a 4.6 mm diameter drop. The A/D sample rate for investigating the acoustical signal from the bubble was 250 kHz. This was necessitated by the limited computer buffer and the delay time between drop impact and bubble formulation. The maximum delay time for the largest drop size investigated was approximately 63 ms. This forced a choice of a 128 ms record length since the next smaller record length was 64 ms. A choice of 64 ms would have resulted in truncating some of the bubble signals

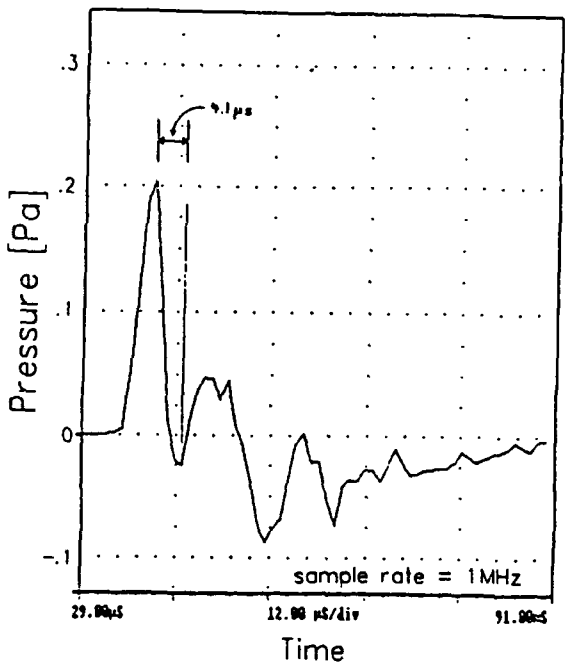

Figure 3.4: Impact signal from 4.6 mm drop

Figure 3.5: Sketch of 4.6 mm drop profile

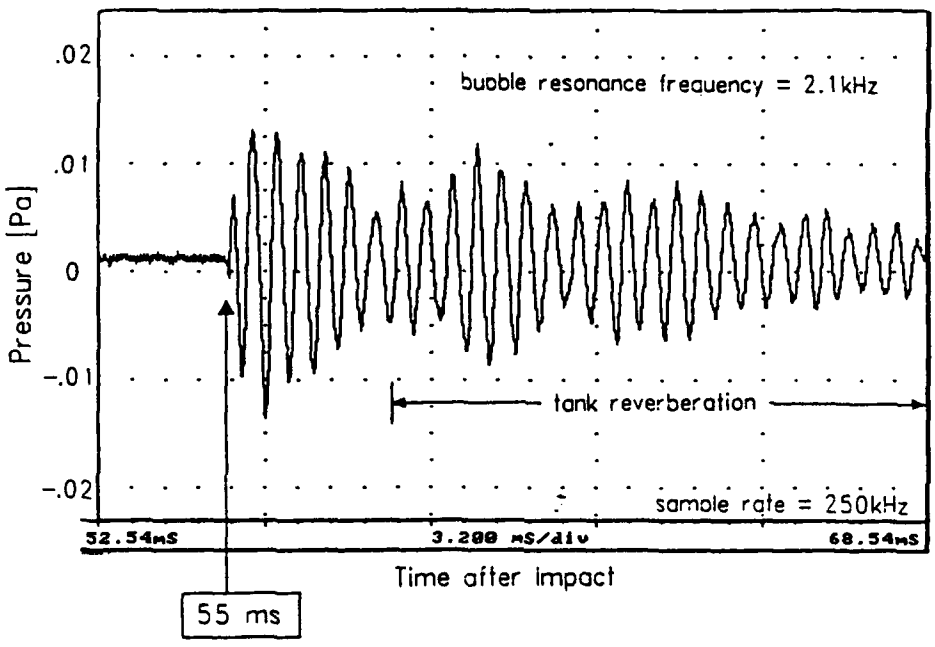

Figure 3.6: Bubble signal from 4.6 mm drop

from larger drops. The data storage buffer was limited to 32 Kbytes, thus giving a sampling period of 4 μs or a sampling frequency of 250 kHz. As shown in Figure 3.7, this delay time is a function of drop diameter and increases as drop diameter is increased. An explanation for the dependence of delay time on drop diameter is suggested by photographic results presented in the following chapter.

The final 10 ms of the bubble signal shown in Figure 3.6 is annotated as tank reverberation from bottom and side walls of the tank. The reverberation was the inescapable result of conducting the experiment in a tank of 1.4 m diameter and 1.3 m depth with no anechoic properties. This was not a significant problem since it did not preclude the determination of impact to bubble delay time, bubble damping characteristics or bubble frequency.

As discussed in the background section, Type I drops create bubbles 100% of the time at normal incidence to a flat water surface. This makes these drops

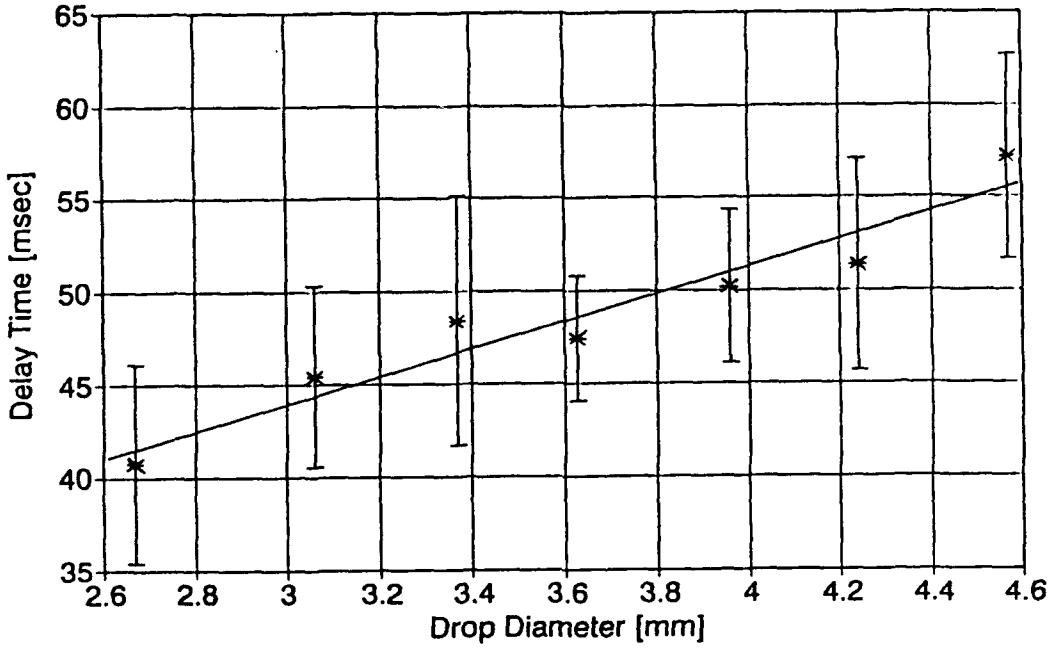

Figure 3.7: Bubble delay time

more significant from an acoustical point of view than other drops in the 0-2 mm size range. In order to evaluate the acoustical significance of Type II drops, their propensity to generate bubbles must be determined. Figure 3.8 shows the percentage of drops which create bubbles versus drop diameter. The shape of this plot suggests that drops with a diameter in the vicinity of 4 mm are the major contributors to the acoustical signal from Type II drops. As drop size decreases, the likelihood of bubble formation falls off rapidly. At diameters below 2.7 mm, bubble formation is extremely sporadic (<10%). This, in fact, was the basis for establishing the lower bound for Type II drops at 2.7 mm. The relationship between bubble formation and drop diameter for Type II drops shown in Figure 3.8 suggests that there is a difference between the bubble creation mechanism of Type I and Type II drops. If the mechanisms were identical, then one would expect to find a similar relationship between bubble creation and drop diameter for both Type I and Type II drops. This

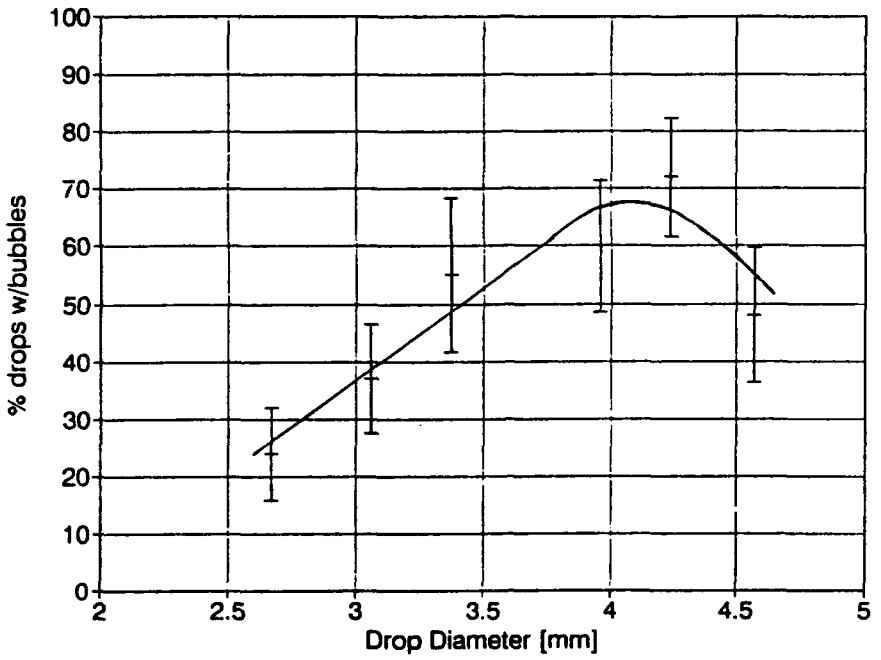

Figure 3.8: Bubble Creation Percentage (% Drops with Bubbles vs. Drop Diameter)

is clearly not the case since Type I drops create bubbles 100% of the time. This initial reasoning was supported later by the photographic evidence.

D. SPECTRAL CHARACTERISTICS OF THE ACOUSTICAL SIGNATURE

Both the impact signal and the bubble signal contribute to the spectral characteristic of the underwater acoustical signature of a drop. The duration of the bubble signal (when present) is much greater than the duration of the impact signal. This is a critical point. The frequency component due to the bubble will dominate the component due to the impact since it has greater energy and a relatively narrower frequency band. A quantitative analysis of bubble energy and total acoustical energy from the drop is to be presented in a companion thesis (Jacobus, 1991).

The spectral characteristics of the impact were initially investigated based on the hypothesis that the spectral peaks, due to the impact, would shift with change in drop diameter. The impact produces acoustic energy in two loosely definable spectral regions. Figures 3.9 and 3.10 show the spectrum of an impact signal for a Type II drop with a bandpass filter of 1-300 kHz at two different resolutions. The lower frequency region (5-35 kHz) consists of two groups of three or four individual peaks. The second group is always lower in amplitude than the first. Comparison of the frequency spacing of peaks comprising the first and second group does not quantitatively support a harmonic relationship between the two. However, the consistent appearance of these spectral groupings with the same relative amplitude difference suggests that they may be generated by non-linear mechanisms in the impact event. The higher frequency region is centered roughly at 90 kHz and is always quite broad with a bandwidth of $\sim$ 40 kHz. This region may be directly related to the period of the secondary and tertiary peaks which follow the initial peak at impact (see Figure 3.3). The periodicity of these peaks ranges between 10 and 11 μs, which would give a frequency range of 91-100 kHz. Although these observations may add to the understanding of the physical process occurring in the impact, they may be of minimal significance in the total underwater acoustics picture. Higher frequencies will not propagate far enough to be of interest unless monitored by a near surface, localized hydrophone. Spectral peaks of lower frequencies (5-35 kHz) do not provide a fixed signature characteristic for a given drop size. Therefore, the impact acoustical signature does not provide a method of clearly identifying a specific drop size.

For a significant percentage of drops, 40 to 55 ms after the impact, there is acoustical radiation attributable to bubble oscillations. Occasionally, there is more than one bubble, the later oscillations being weaker than the original. The

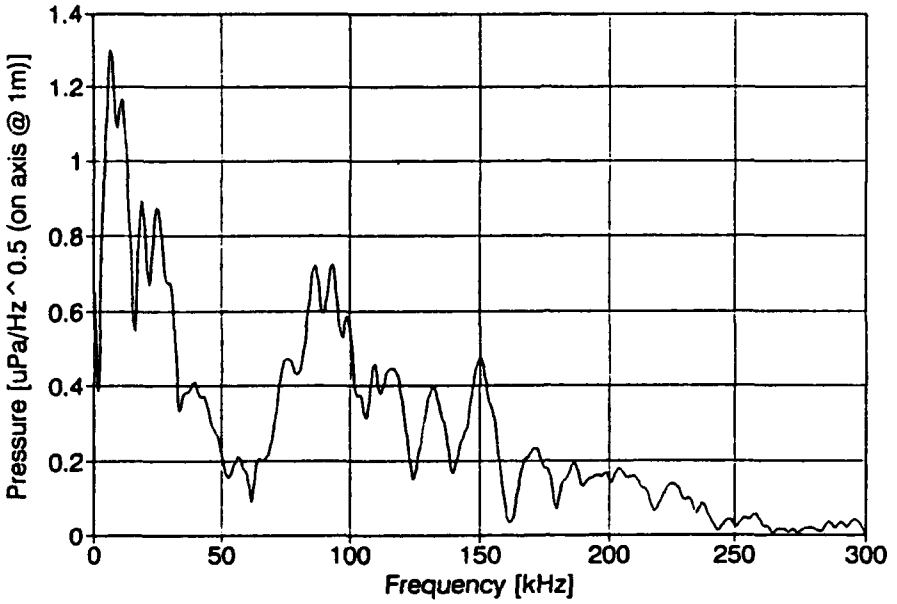

Figure 3.9: Typical Impact Spectrum (2-300 kHz)

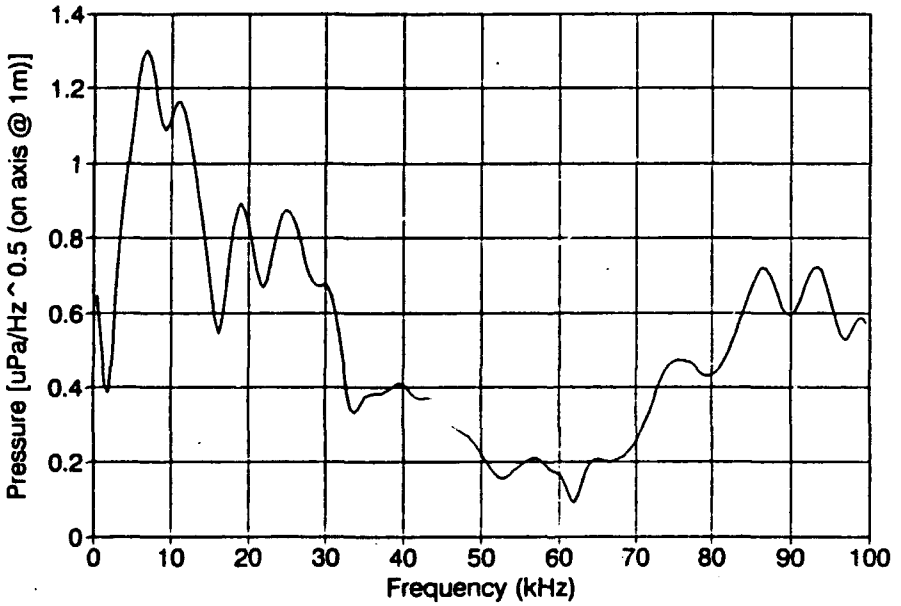

Figure 3.10: Typical Impact Spectrum (2-100 kHz)

largest amplitude oscillation is denoted as the "dominant bubble" signal. It is always lower in frequency than the "secondary" bubbles. The acoustical signature of the dominant bubble shows that a clearly definable frequency shift occurs as drop size is varied. The spectral peak for a bubble is an ideal characteristic for tracking a frequency shift due to its relatively narrow bandwidth. (See Figure 3.11) Data from over 200 drops in the 2.7 to 4.6 mm diameter size range were used to generate the graph of dominant bubble frequencies in Figure 3.12. All bubble signals were processed using an FFT with a uniform record length of 8 ms to ensure a frequency resolution of 125 Hz for all drop sizes. A linear regression with these data gives the following relationship of dominant frequency to drop diameter:

$$\text{Frequency } [kHz] = \frac{175}{\text{diameter}^3\,[\text{mm}^3]} + .74 \tag{3.2}$$

The mass of a drop is proportional to the cube of the drop diameter and the terminal velocity of these drops is approximately constant ($\pm 10\%$). Therefore, based on the relationship between frequency and drop diameter in Equation 3.2, the frequency is approximately proportional to the kinetic energy (K.E.) of the drop as it strikes the water (Figure 3.13).

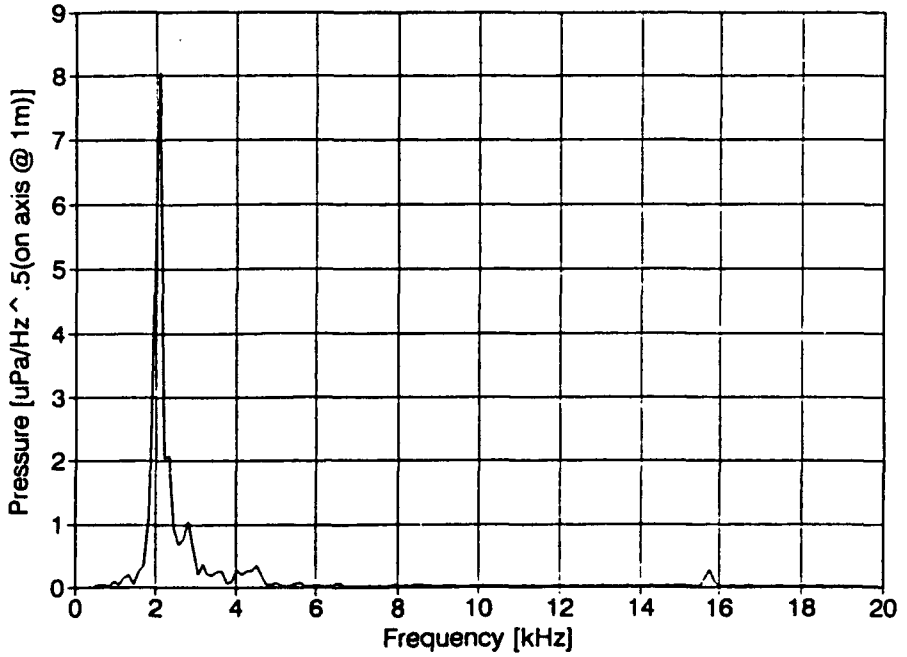

Figure 3.11: Typical Bubble Spectrum (2-20 kHz)

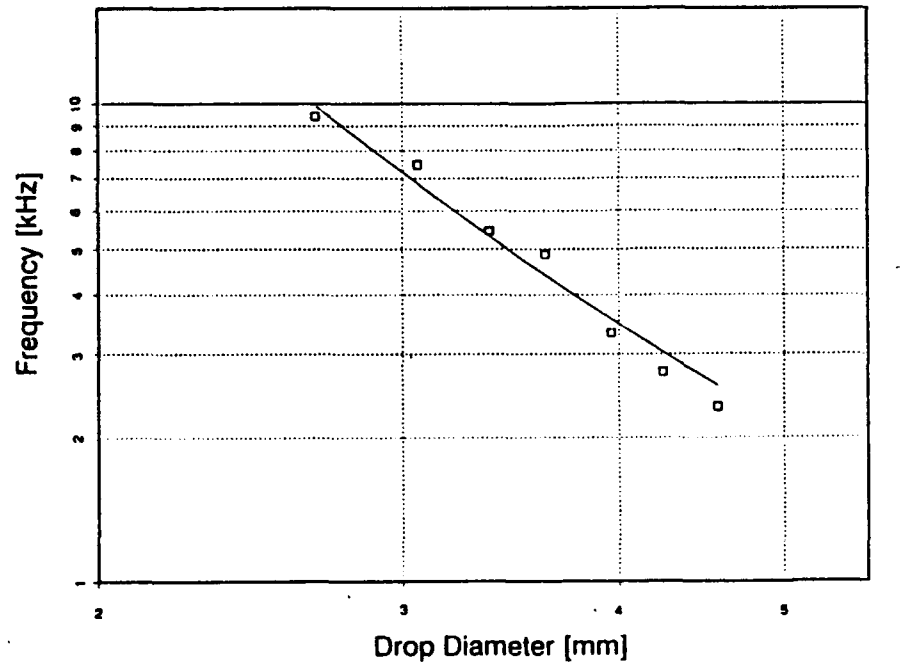

Figure 3.12: Dominant Bubble Frequency vs. Drop Diameter

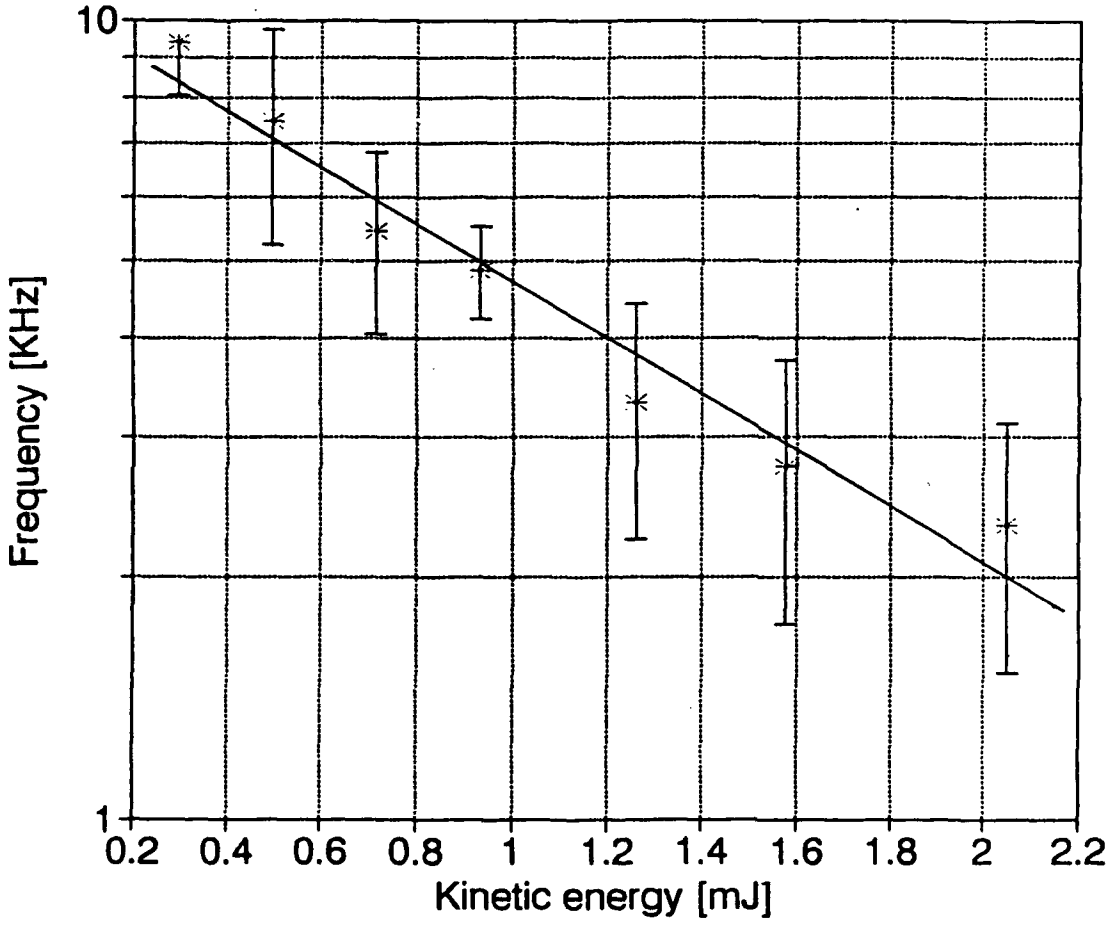

Figure 3.13: Bubble Frequency vs. Drop Kinetic Energy

IV. HIGH SPEED PHOTOGRAPHY EXPERIMENT

In this experiment, the acoustical signal and optical image of a 4.6 mm diameter drop were recorded simultaneously. The objective was to investigate the mechanism of bubble formation by Type II drops. The discontinuity in the size of drops producing bubbles (Figure 1.2) suggested that different physical processes are involved. The acoustical signal was recorded using the set up for the acoustical experiment shown in Figures 3.1 and 3.2 with the following exceptions:

- The hydrophone was placed in a glass aquarium (25 x 50 x 30 cm) mounted on top of the redwood tank.
- The overhead video camera was not used.

The optical image of the drop was recorded using a high speed Milliken movie camera borrowed from the Imaging Technology department of NASA Ames, Moffet Field, CA. A detailed description of the lighting and camera position is included in Appendix A.

Figure 4.1 is a series of sketches which depict principal phases of a 4.6 mm diameter drop impact and subsequent bubble formation. Note that the time interval between frames is not uniform. Only significant changes in the physical geometry of the event are depicted to aid in understanding the bubble production mechanism.

Frame 1 shows the drop just prior to impact. All drops were observed to have this ellipsoidal appearance with a flattened underside. The ratio of horizontal dimension to vertical dimension was $1.4 \pm .1$. This agrees with theoretical predictions of drop shape for similar drop sizes (Pruppacher and Pitter; 1971). It is possible

that some drops are dimpled on the flattened side, but the photographic evidence is not clear.

Frame 2 depicts the formation of a crown 2.5 ms after impact. Many aerosols are ejected from the rim of the crown at this time. At 7.5 ms, the crown has begun to bend in on itself. The hemispherical cavity under the crown is expanding uniformly. Frames 4 and 5 show the crown continuing to close and finally closing at approximately 15 ms to form a closed canopy.

As the hemispherical cavity continues to grow, water mass is transported upward either along the inside or as part of the canopy. This appears to provide the source of water mass that forms the upward moving jet shown in Frame 6. This jet reaches a mean height of 2.9 $\pm$ .3 cm in approximately 25-30 ms.

In Frame 7, the upward moving jet has reached its maximum height. At this point, a downward plunging jet is formed. This jet continues to move downward in Frame 8, but has developed a noticeable cant. This appears to be the condition at which one can distinguish between a drop that produces a bubble and one that does not. Drops that produce bubbles always have a cant in their downward moving jet. Drops that do not produce bubbles seem to have a more symmetrical jet motion which plunges roughly straight down. Also in Frame 8, notice that the bottom of the hemispherical cavity has begun to flatten. This flattening and rising of the bottom of the cavity continues throughout the rest of the event while the diameter of the cavity remains relatively constant at its maximum diameter. The value of the maximum diameter is 2.7 $\pm$ .1 cm.

In Frame 9, the downward moving jet punctures the cavity and pushes through carrying with it gas from the enclosed region between the canopy and the cavity. When the jet retracts back into the cavity, a portion of the vapor remains behind and forms a volume that begins to oscillate almost immediately. These oscillations

damp down in 5-8 ms for the largest bubble size. The theoretical damping period for this bubble size is 5.1 ms.

For drops that do not produce bubbles, Frames 8 and 9 would show a jet plunging straight down as previously mentioned. Frame 10 would show that the jet has retracted but no gas volume is left behind. It is clear that whatever reasoning one chooses to explain the formation/non-formation mechanism, it must include the canted jet versus straight jet observation. The image of the jet on film is not clear enough to discern the transport mechanism for the gas into the water volume. As the gas volume enters the water, buoyant forces would tend to push up on it, for a canted jet this would provide it the force necessary to break off. In the case of the straight vertically oriented jet, the buoyant forces would simply push gas volume and jet back up into the cavity, leaving no gas volume behind.

The velocity of the downward moving jet was estimated using the change in vertical position over three to four frames. This proved to be of little value since the variation in cant angles of the jet make determination of velocity impossible without additional information which is unavilabile from the present photographic data.

Figure 3.7 in Chapter III shows the variation in delay time between impact and dominant bubble formation with respect to drop diameter. From Figure 4.1, this variation in delay time is apparently due to scaled changes in the physical dimensions of the cavity and canopy. Regrettably, there is no photographic evidence to support this conclusion at this time because only the largest drop size was photographed. However, it seems unlikely that there could be any other logical explanation.

The term dominant bubble has been used in the previous chapter to distinguish between the single, low frequency (2-10 kHz), high energy bubble and multiple, higher frequency (15-25 kHz) low energy bubbles. This distinction became necessary as a result of photographic evidence of these small "secondary" bubbles formed after

the dominant bubble. Secondary bubbles are not always formed when a dominant bubble is created and they are never formed if dominant bubble is not present.

Photographic evidence combined with the Frequency vs. Kinetic Energy relationship of Figure 3.13 suggests that there is a physical connection between drop K.E. and the size of the gas volume transported into the water by the downward plunging jet. One hypothesis is that greater K.E. creates a higher velocity jet which is capable of transporting a greater volume of gas into the water, thus forming a larger bubble. A parallel line of reasoning suggested by Figure 3.12 is that the greater mass of larger drops contributes more water mass to the jet and thus allows it to carry more gas forming a larger, lower frequency bubble.

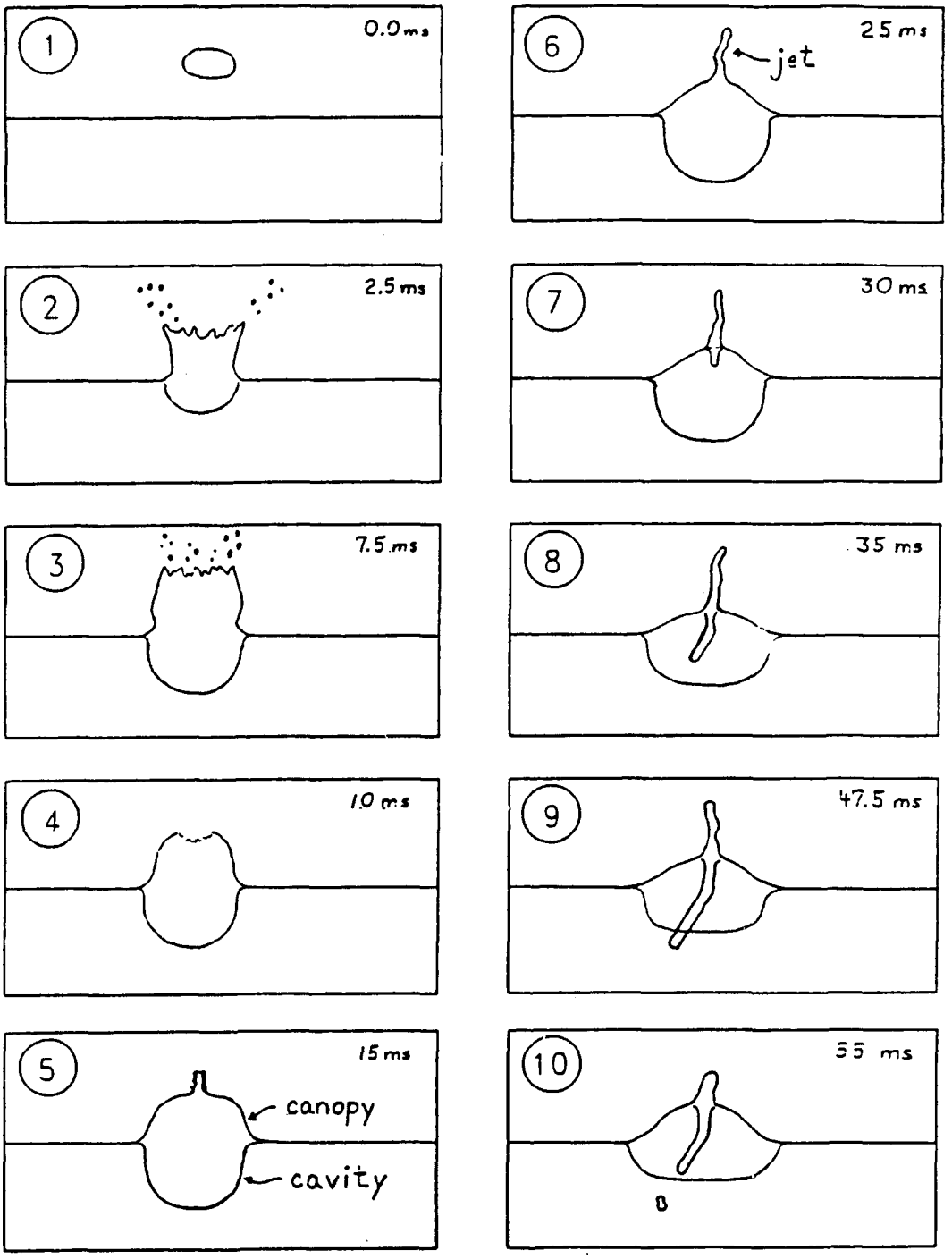

Figure 4.1: Drop Sequence Sketch

V. CONCLUSIONS

The motivation driving the research for this thesis was the search for an underwater acoustical characteristic related to raindrop size. It is hoped that such a characteristic may be exploited to determine, acoustically, the drop size distribution in a rainstorm over open water. As a result of this research, the following conclusions were reached.

- Previous research which used non-terminal velocity large drops to simulate raindrops of 2-5 mm diameter was in error. Our research shows that terminal velocity is necessary in order for laboratory drops to produce bubbles by the same mechanism as actual large raindrops.

- There are notches which modulate the impact acoustical signal for large drops. The timing of these notches suggests interference between the impact pressure pulse and a reflected pulse within the drop volume.

- There is a clearly quantifiable relationship between drop size and frequency of the dominant bubble produced for the range of drop sizes investigated in this thesis. This range was 2.7-4.6 mm in diameter with a bubble frequency from 10 - 2 kHz, respectively.

- The percentage of bubbles created by large drops is not sporadic or irregular as stated in previously published research. The percentage is quantifiable with a peak production of approximately 65% at 4 mm diameter. There are essentially no bubbles for 1.2-2.0 mm diameter drops. The bubble percentage

depends on the flow dynamics of the jet action in the canopy and cavity created by drop impact.

The last two conclusions give a qualitative feel for the underwater acoustic energy spectrum of large rain drops. The peak energy level should be between 2 and 4 kHz with a decrease in energy level as frequency approaches 10 kHz. This decrease will be mitigated somewhat by the increase in drop numbers for smaller size (higher frequency) drops. With a more quantitative description of the energy spectrum, it should be possible to predict drop size distribution by monitoring the underwater acoustic signal of rain. This will result in an excellent estimation of rainfall rate.

APPENDIX A
High Speed Motion Analysis of a Water Drop

BROOKS INSTITUTE CONTACTS: Dominic Hart and Mark Mattivi

DATE OF EXPERIMENT: 12 October 1990

LOCATION OF EXPERIMENT: Naval Postgraduate School, Monterey, CA

PURPOSE OF THE EXPERIMENT: To document the acoustical and optical image formed by a water drop at terminal velocity.

OPTICAL EQUIPMENT USED:

- Camera: Milliken high-speed intermittent type camera
- Shutter opening: 7 degree shutter
- Frame rate: 400 fps
- Film type: KODAK 7292 color negative

LIGHTING EQUIPMENT:

- LOWEL quartz halogen tungsten lighting
- 2 diffusion flats
- Black GOBO cards

PROCEDURE:

1. An initial overview was completed of the test shaft and area. The decision was made to utilize a bright field type of illumination due to the high shutter speed and a need to record detail in the test subject (water drop).

2. An initial exposure reading was taken using an incident exposure meter. The exposure was set at 1/19000 sec @ F2.8.

3. The camera was positioned on axis with the water line of the tank at mid-frame. The field of view was determined to be 5.5 x 5.5 inches.

4. Depth of field for the subject was measured. Our measurements concluded that we had a 2.5 inch depth of field from fore/back ground of the subject.

5. The focus for the Milliken camera was confirmed by rotating the shutter to the open position and installing the bore-sight into the camera. The focal length of the bore-sight was adjusted by focusing onto the ground glass field. The focus of the taking lens was then adjusted until the subject was sharp. Focus was secured by taping the focus ring of the taking lens into place. The aperture was also taped in place.

6. The water drop was dropped a distance of 85 feet down a vertical ventilation shaft. An eye dropper was used to form the drop and positioning was accomplished manually. Release of the drop was relayed by intercom using a count procedure.

7. Camera start-up was manually triggered one second into the drop sequence. This allowed the camera to come up to a steady frame rate prior to the drop entering the field of view.

8. The camera was shut down approximately one second after impact of the drop in the tank.

EXPOSURE DATA: 1/19000 sec @ F2.8.

TEST OBSERVATIONS:

- The release and accuracy of the impact of the water drop seems to be the weakest link in the test procedure.
- Isolation of the shaft from air drafts and currents could potentially improve the accuracy of the impact.
- If the introduction of a dye/fluorescein into the drop does not change the physical characteristics of the drop, it is recommended. The introduction of such a "marker" into the drop mass would enhance the ability to track the water mass of the drop throughout the impact cycle.

ANALYSIS AND CONCLUSIONS:

The initial review of the 1000 feet of film ran during 48 test runs revealed new optical data of the requested event.

There are several post-experiment observations which suggest possible improvements and modifications of the photographic technique described above.

1. A faster camera frame rate to increase the time magnification factor. This would allow discrete portions of the event to be analyzed in more detail.
2. Still photographic analysis of the event using a repeatable trigger and delay unit. A still image would be of higher quality with better focus and depth of field.

3. Introduce dye into the drop to allow for motion trace analysis.

Overall, this test procedure was completed with very little error. The optical data retrieved met or exceeded the expectations of the test goal.

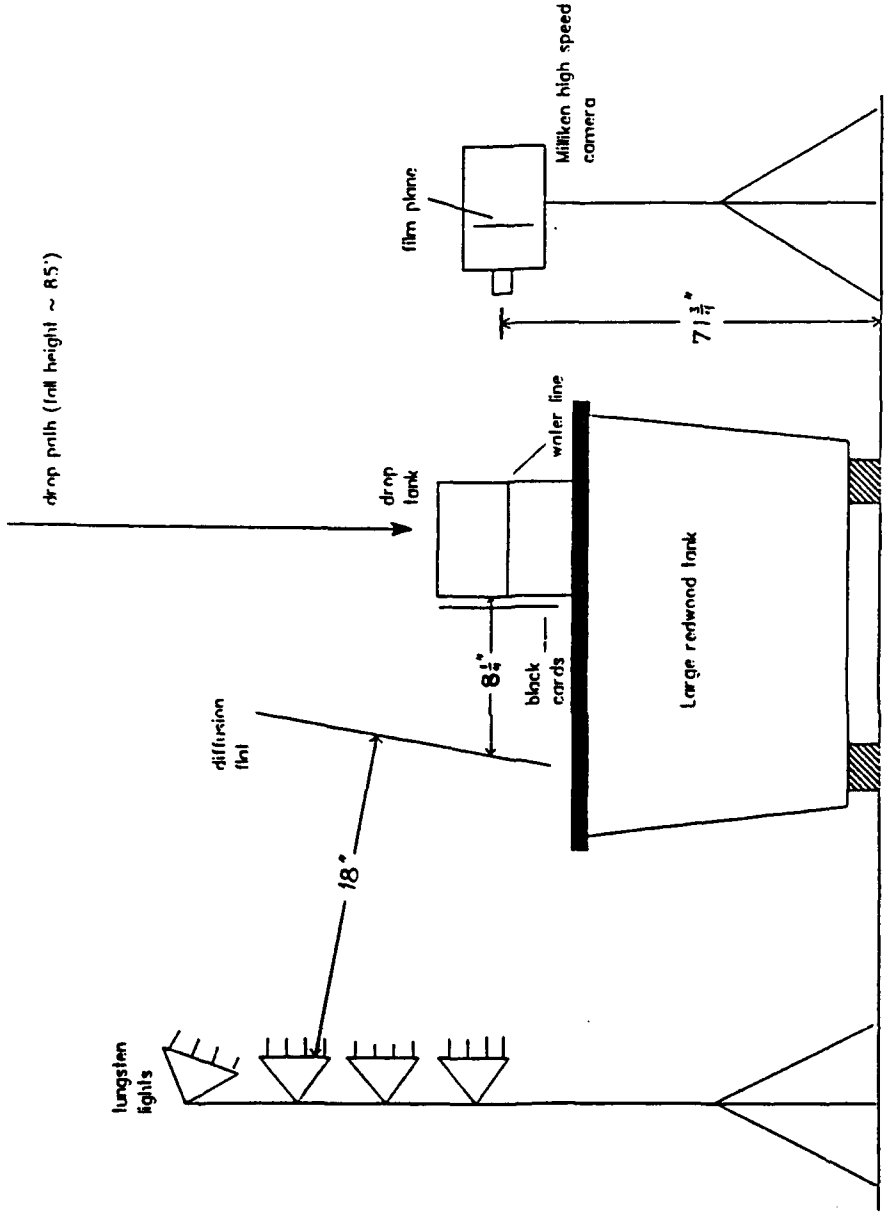

Figure A.1: Photographic/lighting set-up (Side View)

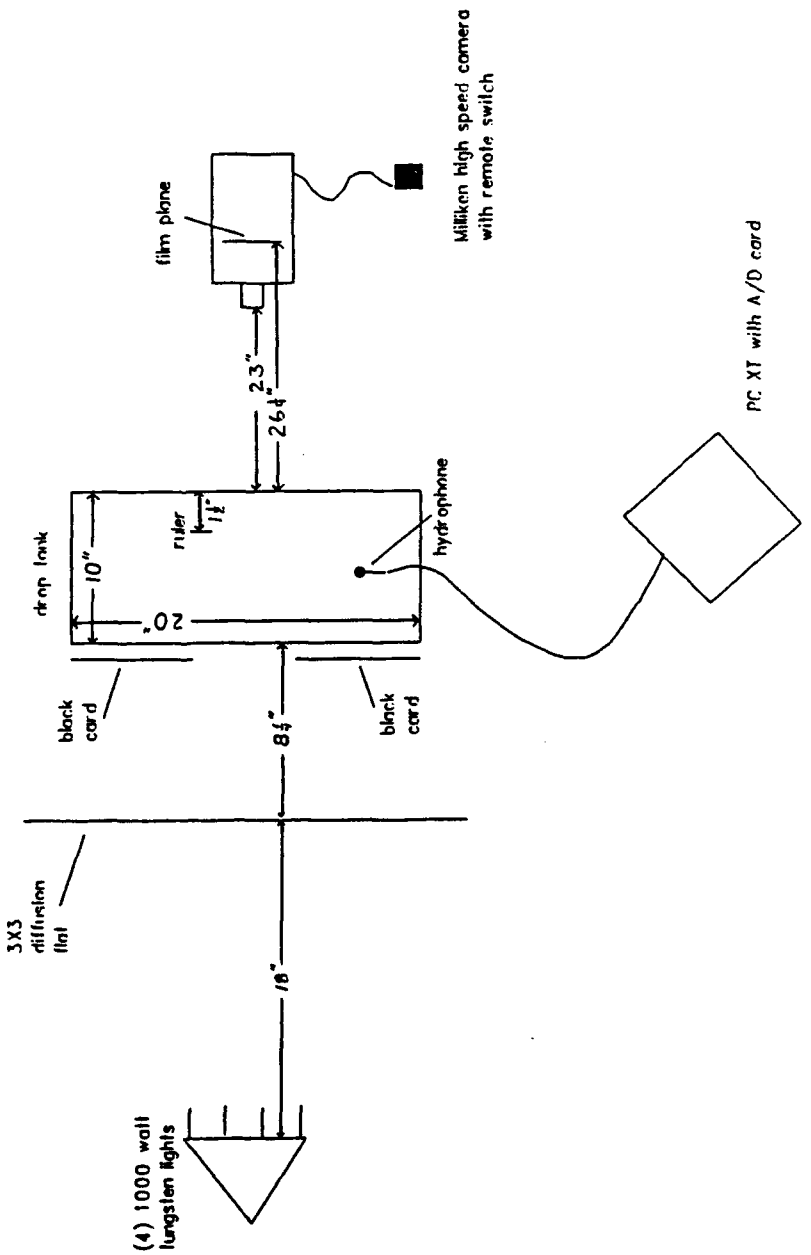

Figure A.2: Photographic/lighting set-up (Top View)

LIST OF REFERENCES

1. Franz, G., "Splashes as sources of sound in liquids", *J. Acoust. Soc Am.* **31**, pp. 1080-1096, 1959.

2. Heindsman, T. E., Smith, R. H. Smith and Arneson, A.D., "Effect of rain upon underwater noise levels", *J. Acoust. Soc. Am.*, **27**, pp. 378-379, 1955.

3. Kurgan, A., "Underwater sound radiated by impacts and bubbles created by raindrops", M.S. Thesis, Naval Postgraduate School, Monterey, CA 93943, 1989.

4. Longuet-Higgins, M.S., "An analytical model of sound production by raindrops", *J. Fluid Mech.*, **214**, pp. 395-410, 1990.

5. Medwin, H., Kurgan, A., and Nystuen, J. A., "Impact and bubble sound from raindrops at normal and oblique incidence", *J. Acoust. Soc. Am*, **88(1)**, pp. 413-418, 1990.

6. Nystuen, J. A., "Rainfall measurements using underwater ambient noise", *J. Acoust. Soc. Am.*, **79**, pp. 972-982, 1986.

7. Nystuen, J. A., "An explanation of the sound generated by light rain in the presence of wind", to appear in *Natural Physical Sources of Underwater Sound*, Kerman, B. R., ed., Kluwer Academic Press, 1991.

8. Nystuen, J. A. and Farmer, D. M., "Precipitation in the Canadian Atlantic Storms Program: Measurements of the Acoustic Signature", *Atmosphere-Ocean*, **27**, pp. 237-257, 1989.

9. Oguz, H. N. and Prosperetti, A., "Bubble entrainment by the impact of drops on liquid surfaces", *J. Fluid Mechanics*, **218**, pp. 143-162, 1990.

10. Pumphrey, H. C., Crum, L. A., and Bjorno, L., "Underwater sound produced by individual drop impacts and rainfall", *J. Acoust. Soc. Am*, **85**, pp. 1518-1526, 1989.

11. Pruppacher, H. R., and Klett, J. D., *Microphysics of Clouds and Precipitation*, D. Reidel Publishing Company, Dordrecht, Holland, 1978.

12. Pruppacher, H. R. and Pitter, R. L., "A Semi-Empirical Determination of the Shape of Cloud and Rain Drops", *J. Atmos. Sci*, **28**, pp. 86-94, 1971.

13. Scrimger, J. A., Evans, D. J., McBean, G. A., Farmer, D. M., and Kerman, B. R., "Underwater noise due to rain, hail, and snow", *J. Acoust. Soc. Am.*, **81**, pp. 79-86, 1987.

14. Scrimger, J. A., Evans, D. J., and Yee, W., "Underwater noise due to rain - Open ocean measurements", *J. Acoust. Soc. Am.*, **85**, pp. 726-731, 1989.

15. Ulbrick, C. W., and Atlas, D., "The rain parameter diagram: Methods and applications", *J. Geophys. Res.*, **83**, pp. 1319-1325, 1978.

INITIAL DISTRIBUTION LIST

		No. of Copies
1.	Defense Technical Information Center Cameron Station Alexandria, VA 22304-6145	2
2.	Library, Code 52 Naval Postgraduate School Monterey, CA 93943-5002	2
3.	Department of Physics Attn: Professor H. Medwin, Code PH/Md Naval Postgraduate School Monterey, CA 93943	3
4.	Department of Physics Attn: Professor A. A. Atchley Naval Postgraduate School Monterey, CA 93943	2
5.	Department of Oceanography Attn: Professor J. A. Nystuen, Code OC/Ny Naval Postgraduate School Monterey, CA 93943	1
6.	Dr. Marshall Orr Office of Naval Research (Code 11250A) 800 N. Quincy Street Arlington, VA 22217	1
7.	Mr. Harry Selsor NOARL, Code 311 Stennis Space Center Mississippi 39529-5004	1

8. Lt. David E. Snyder — 1
c/o Carl E. Snyder
628 Gordon Rd
Moreland, GA 30259

10. Department of Physics — 1
Attn: Lt. Pete Jacobus
Naval Postgraduate School
Monterey, CA 93943

11. Brooks Institute of Photography — 1
Attn: Mark Mattivi / Dr. Vern Miller
320 Santa Cruz
Santa Barbara, CA 93109